Single-electrolyte isotachophoresis : on-chip analyte focusing and separation

Quist, J.W.

Cover Page

The handle http://hdl.handle.net/1887/24857 holds various files of this Leiden University dissertation

Author: Quist, Johannis Willem
Title: Single-electrolyte isotachophoresis : on-chip analyte focusing and separation
Issue Date: 2014-03-20

3 Single-Electrolyte Isotachophoresis Using a Nanochannel-Induced Depletion Zone

Isotachophoretic separations are triggered at the border of a nanochannel-induced ion-depleted zone. This depletion zone acts as a terminating electrolyte and is created by concentration polarization over the nanochannel. We show both continuous and discrete sample injections as well as separation of up to four analytes. Continuous injection of a spacer compound was used for selective analyte elution. Zones were kept focused for over one hour, while shifting less than 700 µm. Moreover, zones could be deliberately positioned in the separation channel and focusing strength could be precisely tuned employing a three-point voltage actuation scheme. This makes depletion zone isotachophoresis (dzITP) a fully controllable single-electrolyte focusing and separation technique. For on-chip electrokinetic methods, dzITP sets a new standard in terms of versatility and operational simplicity.

Isotachophoresis (ITP) is a powerful electrokinetic technique for the concentration, separation, purification, and quantification of ionic analytes, especially when downscaled to microfluidic devices.[1, 2] In 1998, Walker et al. were among the first to demonstrate on-chip ITP using Raman spectroscopy to detect herbicides.[3] Kanianski et al. coupled ITP to capillary electrophoresis (CE) on a chip and showed isotachopherograms of up to 14 analytes.[4] Several

reports describe over 10,000-fold concentration.[5-7] Jung et al. even reported millionfold sample stacking using transient ITP.[8] Miniaturized ITP is applicable to a broad range of samples, including toxins from tap water,[9] explosive residues,[10] proteins,[11] DNA from PCR samples,[12, 13] nucleic acids from whole blood,[14] and small RNA molecules from cell lysate.[15] Hybridization of RNAs with molecular beacons by ITP[16] was applied to bacterial rRNAs from urine,[17] demonstrating the potential of on-chip ITP for biochemical assays. A major recent achievement was the integration of an ITP chip and laser-induced-fluorescence (LIF) detection into a single hand-held device.[18] Nevertheless, ITP has still to come to its full potential, as until now it has not been widely used for bioanalytical applications.[19-21] A major limitation is that ITP requires a sample to be injected between a leading electrolyte and a terminating electrolyte. Compared to, e.g., capillary electrophoresis (CE), which uses a single electrolyte only, handling and method development is not straightforward. Another limitation of conventional ITP is that analyte zone positions are difficult to control. This is due to the different conductivities of the ITP zones, resulting in continuous changes of electric field distributions during electromigration. Several stationary ITP strategies have been developed to alleviate this limitation. One such strategy employs a hydrodynamic counterflow, but this has the disadvantage of dispersion due to a parabolic flow profile.[22] A more elegant strategy is balancing the electrophoretic motion of the ITP zones by an opposite electro-osmotic flow (EOF).[23-26] However, with this method it is still complicated to change analyte zone positions in a controlled manner without changing pH or electrolyte concentrations.

In this paper we overcome the mentioned limitations by a radically different approach which combines the strengths of on-chip ITP with the merits of nanofluidic concentration devices.[27, 28] These devices, which have been extensively reviewed by Kim et al.,[29] are in fact miniaturized variants of electrocapture devices. Electrocapture is a powerful method which utilizes capillaries with perm-selective membrane junctions for trapping and selective release of ionic compounds.[30, 31] In nanofluidic concentration devices, at least two parallel microchannels are connected by a nanochannel, over which an electric field is applied (Figure 1a). Asymmetric distribution of anions and cations[32, 33] makes the nanochannel perm-selective, leading to concentration polarization.[34-36] This causes the formation of a depletion zone in the anodic microchannel. A tangential EOF through this microchannel transports analytes toward the border of the depletion zone, where they are trapped (Figure 1b). Various groups have investigated devices based on similar principles,[37-43] showing that this has become a very active research field within a short time. Potential applications include immunoassays,[44-47] enzyme assays,[44, 48, 49] massive parallelization,[50, 51] and desalination.[52] Here we employ a depletion zone to induce isotachophoretic separations. To our knowledge, this is the first time such separations are demonstrated in nanofluidic concentration devices. Depletion zone isotachophoresis (dzITP), as we coin this novel approach, is performed with a single electrolyte only. A three-point voltage actuation scheme gives complete control over the position of the zones and the sharpness of their borders, utilizing the fact that the method is quasistatic. The simplicity and versatility of our method makes it a powerful new tool in the electrokinetic focusing and separation toolkit.

Experimental Section

Chemicals

Lithium carbonate was obtained from Acros Organics (Geel, Belgium), disodium fluorescein was obtained from Riedel-de Haën (Seelze, Germany), 6-carboxyfluorescein was obtained from Sigma-Aldrich (Steinheim, Germany), and sodium acetate was obtained from Merck (Darmstadt, Germany). FITC-labeling of glutamate and leucine was performed as follows. To 0.5 mmol of amino acid an aqueous solution of potassium hydroxide, 1 g/ml, was added in a 1:1 weight:volume ratio, followed by addition of 1 ml of ethanol. Under vigorous stirring on ice, a suspension of FITC in ethanol (1 mol/L) was added to the amino acid in a molar ratio of 1:1; together with 1 ml 0.5 mol/L potassium hydroxide and 0.5 mL ethanol. This mixture was left on ice to react for 2 h in the dark under continued stirring. Purification of the reaction product was performed using a Gilson preparative HPLC system (Gilson, Inc., Middleton, USA) equipped with a Phenomex Gemini C18 column, 15x21 mm, 5 micron (Phenomenex, Torrance, USA) using an acetonitrile/water (10 mmol/L ammonium acetate, pH=8) gradient. Purity of compounds was established with LC-UVMS and CZE-LIF and found to be > 99%. After freeze-drying, each purified FITC-amino acid was dissolved in dimethyl sulfoxide (DMSO), 1.0 mmol/L, and stored at -80°C awaiting experiments.

In all experiments, 2.0 mmol/L lithium carbonate, pH 10.6, was used as the background electrolyte. Solutions were prepared fresh before experiments.
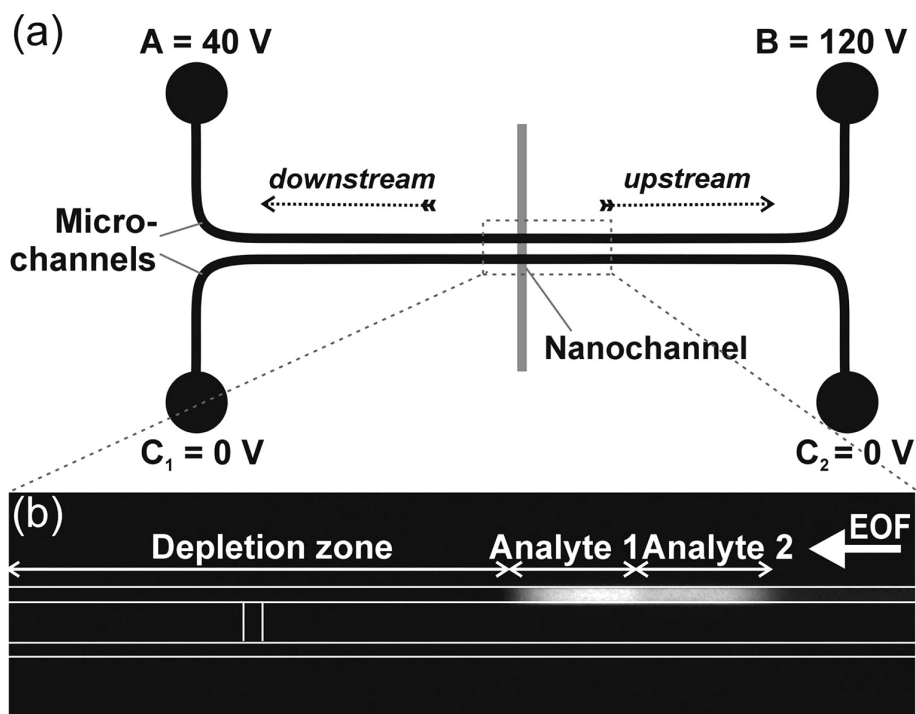
Figure 1. (a) Chip layout consisting of two microchannels and one nanochannel. An example of three-point voltage actuation is provided: A is the downstream voltage and B the upstream voltage, while the lower channel is connected to ground, as represented by voltages $C_{1,2}$ = 0 V. Downstream and upstream directions are indicated by dashed arrows. (b) Example of dzITP separated zones. The channel contains a depletion zone that extends mostly in the downstream channel. Analytes focus at the border of the depletion zone and order themselves in clearly distinguishable zones. Lines that indicate micro- and nanochannels were drawn onto the CCD images.

Chip Fabrication

Chips were fabricated in Pyrex wafers using standard lithography techniques and deep reactive ion etching (DRIE). Photoresists (SU 8-10 and ma-P 1275) and developers (mr-Dev 600 and ma-D 331) were obtained from Microresist Technologies (Berlin, Germany). Nmethylpyrrolidone (NMP) was obtained

from Rathburn Chemicals (Walkerburn, Scotland). AbsorbMaxTM film, fuming nitric acid (100%) and hexamethyldisilazane (HMDS) were obtained from Sigma-Aldrich (Steinheim, Germany). Chips containing micro- and nanochannels were fabricated in 4" Pyrex® wafers (Si-Mat, Kaufering, Germany). The wafers were spin coated with SU 8-10; the wafer was first accelerated to 500 rpm in 5 seconds to allow resist spreading, directly followed by an acceleration to 2000 rpm in 5 seconds, which was maintained for 30 seconds. After spin coating, the resist was allowed to settle for 8 hours at room temperature, after which the resist was prebaked using a hotplate by controlled heating to 95°C in 8 minutes, followed by ambient cool down. The resist was exposed at 6 mW/cm2 for 25 seconds in a Suss MA 45 mask aligner (Karl Suss KG, München-Garching, Germany) in which a Hoya UV34 filter (LG optical, Churchfield, UK) was installed to prevent SU 8 T-topping. During exposure AbsorbMax film was attached to the back side of the wafer, to prevent undesired reflections. The microchannel pattern was transferred using a 5" chromium mask (Delta Mask, Enschede, The Netherlands). A post-exposure bake was done by controlled heating to 95°C in 8 minutes, followed by ambient cool down. Development was done for 3 minutes in mr-Dev 600 developer followed by washing in isopropanol and demineralized water. Using the developed SU 8 resist as a mask, microchannels were etched into the glass wafers by a 1 hour deep reactive ion etching (DRIE) step. DRIE was performed in an Oxford Plasmalab 90+ parallel plate reactor (Oxford Instruments, Abingdon, United Kingdom) using an argon/SF6 plasma. Gas flows were 20 sccm for argon and 25 sccm for SF6. After establishing a stable plasma at 10 mTorr, pressure was set at 2 mTorr. Forward power was 200W. After etching, the SU 8 resist was stripped by placing the wafers in NMP for several hours at

70°C, followed by removal of remaining particles in a fuming nitric acid bath. The wafers were rinsed in water, spin-dried, and baked for 5 minutes at 110°C for dehydration. The wafers were spin coated with HMDS followed by a curing bake at 150°C for 5 minutes. Next, ma-P resist was spin coated at 1000 rpm for 30 seconds preceded by 10 seconds of acceleration. The resist was prebaked for 5 minutes at 95°C. Transfer of the nanochannel pattern was performed by an exposure step as performed as described above. Development was done with ma-D 331 developer for 5 minutes. To etch the nanochannels, DRIE was performed with same parameters as described above, except for the etch time, which was 100 seconds. The ma-P resist was stripped with acetone. Micro- and nanochannel depths were measured with a Dektak 150 profilometer (Veeco, Tucson, AZ) and by scanning electron microscopy using a FEI NovaTM NanoSEM apparatus (FEI, Hillsboro, OR). Each etched wafer was bonded with a second pyrex wafer. In these wafers, fluidic access holes were ultrasonically drilled using a diamond bit. Both wafers were subsequently cleaned in acetone, piranha acid and nitric acid, followed by a 1 minute dip in KOH. A pre-bond was realized upon application of manual pressure, after which direct bonding was performed in an oven (Model P320, Nabertherm GmbH, Lilienthal, Germany). The temperature was ramped to 600°C in 3 h, which temperature was maintained for 4 h, followed by cooling to room temperature with a rate of 50°C/h. After bonding, wafers were not diced, a whole wafer was used from which a single chip was selected. The microchannels had 1.7 μm depth and 20 μm width. Microchannel lengths between fluid reservoirs and the nanochannel were 0.91 cm. The nanochannel that connected the two microchannels was 60 nm deep, 25 μm wide, and 50 μm long.

Chip Preparation

The chip was prefilled with ethanol to eliminate air trapping, after which the chip was flushed at least 15 min with 100 mmol/L NaOH, 15 min with demineralized water, and 15 min with background electrolyte (2.0 mmol/L lithium carbonate). Fluid replacement and flushing was accomplished by leaving the fluid reservoir at one end of a microchannel empty. A combination of capillary action and evaporation of fluid generated a flow which was sufficient to replace all fluid in a microchannel in approximately 3 min. Reservoirs were washed 3 times after fluid replacement. After flushing, all channels and reservoirs were filled with the background electrolyte (2.0 mmol/L lithium carbonate).

Setup and Microscopy

Access holes were extended with fluidic reservoirs (volume 100 µL) using a custom-build interface that was attached to the chip surface using a vacuum. The fluidic reservoirs were electrically connected using gold electrodes. Two power supplies (ES 0300 045, Delta Elektronika BV, Zierikzee, The Netherlands) were controlled via the analog outputs of an NI USB 6221 data acquisition system using LabVIEW 8.2 software (National Instruments, Austin, TX). For fluorescence microscopy, an Olympus IX71 microscope (Olympus, Zoeterwoude, The Netherlands) was used in combination with an Hamamatsu Orca-ER digital camera and Hokawo version 2.1 imaging software (Hamamatsu Photonics, Nuremberg, Germany). The magnification was 40×. To minimize photobleaching, low lamp intensities were combined with 1.0 s integration times.

Data Processing

Spatiotemporal plots (Figure 2) were composed using MATLAB, by adjoining fluorescence profiles obtained from image sequences that were recorded during the experiments. Fluorescence profiles were obtained by averaging 50 image lines and correcting them for background signal. False colors were assigned to represent fluorescence intensity. Raw CCD images were used in Figure 3. Fluorescence profiles were obtained from the CCD images and were smoothed by averaging over 5 pixels. Slope values were determined at the inflection points of the smoothed profiles and normalized with respect to the maximum intensity value of the corresponding analyte zone. Locations of the edges of the zones were obtained by determining the position of the inflection point relative to the upstream edge of the nanochannel.

Results and Discussion

Device Operation

Figure 1a,b shows the general device operation for dzITP. The upper channel in Figure 1a,b is the separation channel; this is the channel where isotachophoretic zones are formed during the experiment. Three-point voltage actuation is utilized: to each of the access holes of the separation channel a voltage source is connected, while the other channel is connected to ground. Upon voltage application, concentration polarization takes place: an ion depletion zone forms in the separation channel, while in the other channel an ion enrichment zone forms (not shown here, see ref 29). Asymmetric voltage application over the separation channel yields an EOF through this channel. The channel arm between the higher voltage and the nanochannel is referred to as the "upstream channel", while the arm between

the lower voltage and the nanochannel is referred to as the "downstream channel" (see Figure 1a). Downstream, the depletion zone continues to grow until the fluid reservoir is reached. This process sometimes appears to lead to fluctuations during the first 30–60 s of an experiment. In the upstream direction, depletion zone growth becomes balanced by the opposing EOF. When the downstream depletion zone reaches the outlet, the electrical resistance in this channel reaches a more stable value, resulting in a near-stable position for the upstream depletion zone border. At this border, analytes are focused based on a difference in ion density (for detailed theory, see Zangle et al.[35]). Meanwhile, analyte concentration and separation into adjacent zones is achieved according to isotachophoretic principles (see Figure 1b). The depletion zone serves here as a terminating electrolyte, and the background electrolyte takes the function of the leading electrolyte. They define the ionic mobility window of analytes that can be focused. The upper boundary of this mobility window is defined by the mobility of the leading ion in the background electrolyte: analytes with higher mobilities will be transported toward the reservoir. The lower boundary depends on the electric field in the depletion zone, which is very high. For example, Kim et al. measured a 30-fold amplified electric field in the depletion zone.[53] Only analytes with very low mobilities are transported through this barrier by EOF.

As the current setup is based on a glass chip, the channels have a negative surface charge. Consequently, only anions are focused and separated at the depletion zone border. In order to enable focusing and separation of cations, the surface charge of the device should be reversed by applying a surface coating or by choosing a different substrate.

Discrete and Continuous Injections

dzITP is demonstrated for both discrete and continuous injections (see Figure 2a,b). Fluorescein, 50 μmol/L, and 6-carboxyfluorescein, 50 μmol/L, were used as analytes; applied voltages were 120 V (upstream) and 40 V (downstream). For discrete injections, only the separation channel was filled with sample, while remaining channels and fluid reservoirs contained background electrolyte only. This resulted in a 309 pL injection volume, as calculated from the microchannel dimensions. Figure 2a shows that isotachophoretic separation continues until all analytes from the discrete sample are focused, after which the zone widths become constant. Over time, bending points can be observed in the growth rate of the analyte zones, as indicated by the arrows in Figure 2a. These bending points correspond to the exhaustion of fluorescein (arrow I) and 6-carboxyfluorescein (arrow II). Lower mobility compounds are exhausted at an earlier stage than compounds of higher mobility, the reason being that lower mobility compounds have a lower electrophoretic drift to counter the EOF, resulting in a higher net velocity. In continuous injections, the analytes were also placed in the upstream fluid reservoir, providing a practically inexhaustible supply of analytes. Therefore, zone broadening was continuous (see Figure 2b). Clearly, no bends due to analyte exhaustion were present. Zone broadening speed of the lower mobility compound (fluorescein) is higher than that of the higher mobility compound (6-carboxyfluorescein), again due to a higher net velocity. Continuous injections are therefore most advantageous for the extraction and focusing of low-concentration, low-mobility analytes, while discrete injections are useful in the quantitative analysis of multiple analytes.
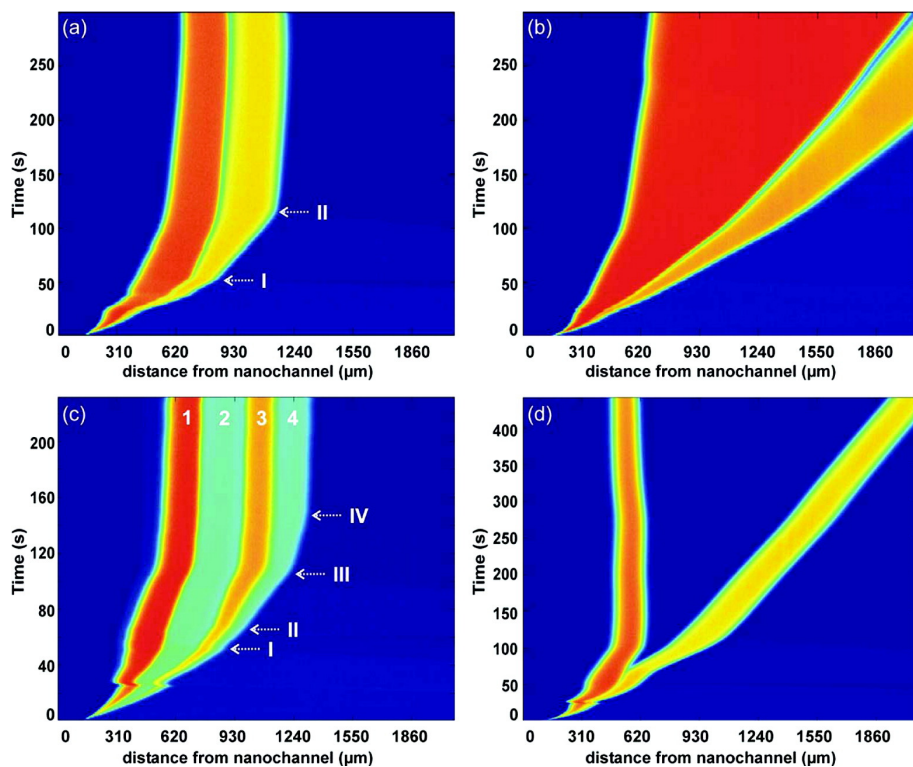
Figure 2. Spatiotemporal plots of dzITP separations. (a) Discrete injection of fluorescein and 6-carboxyfluorescein. Arrows I and II indicate exhaustion of fluorescein and 6-carboxyfluorescein, respectively. (b) Continuous injection of fluorescein and 6-carboxyfluorescein. (c) Discrete injection and separation of four compounds: fluorescein (1), FITC-leucine (2), 6-carboxyfluorescein (3), and FITC-glutamate (4). Arrows I–IV indicate exhaustion of these respective analytes. (d) Discrete injection of fluorescein and 6-carboxyfluorescein combined with a continuous injection of acetate.

Four-Compound Separation

Figure 2c shows concentration and separation of four compounds. A discrete sample containing fluorescein, 6-carboxyfluorescein, FITC-leucine, and FITC-glutamate, 40 μmol/L each, was injected. External voltages were 120 V (upstream) and 40 V (downstream). Within 100 s, four zones of clearly

64

distinguishable fluorescence intensity were formed. Standard addition was used to assign the four zones to each of the four analytes: a doubled concentration of the respective analyte led approximately to a doubling of the width of the corresponding zone (Figure 3). Here, too, bends in the profile coincide with the exhaustion of each of the respective analytes.
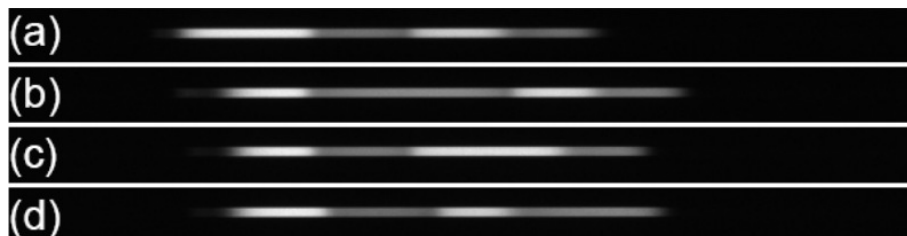

Figure 3. Analyte zone identification by standard addition. In each experiment, the four analytes (fluorescein, FITC-leucine, 6-carboxyfluorescein and FITC-glutamate) were present in concentrations of 30 μmol/L, except for the analyte to be identified, which had a concentration of 60 μmol/L. Discrete injections were performed. From left to right, the four zones were identified as follows: a) first zone: fluorescein; b) second zone: FITC-leucine; c) third zone: 6-carboxyfluorescein; d) fourth zone: FITC-glutamate

Spacer Compounds

A combination of a continuous and a discrete injection is shown in Figure 2d. The upstream fluid reservoir was filled with electrolyte containing 100 μmol/L sodium acetate as a spacer compound, but no analytes. The separation channel was filled with electrolyte containing 30 μmol/L of both fluorescein and 6-carboxyfluorescein as analytes, but no spacer compound. External voltages were 120 V (upstream) and 40 V (downstream). Initially, fluorescein and 6-carboxyfluorescein are focused in adjacent zones. After 70 s, acetate, which has an ionic mobility in between that of fluorescein and 6-carboxyfluorescein, arrives and spaces the two compounds. The fluorescein zone remains focused at the depletion zone border, while the 6-

carboxyfluorescein zone is pushed away in upstream direction by the continuously broadening acetate zone. Spacer addition enables baseline separation of fluorescent compounds enabling more precise identification and quantification. Furthermore, a single compound or a specific group of compounds can be selectively transported away from the depletion zone and can eventually be eluted from the system, while other compounds remain at their near-stationary position at the border of the depletion zone. Advantageously, all compounds remain focused during this process. Thus, spacer addition is a powerful method for purification and transport.

Positional Stability

A crucial feature of dzITP is the positional stability of the depletion zone border. A near-stationary condition is reached after a rather short period, typically on the order of 100 s (see Figure 2), in which depletion rate and EOF velocity reach a balance. A discrete injection experiment was performed with 50 µmol/L of both fluorescein and 6-carboxyfluorescein; external voltages were 120 V (upstream) and 40 V (downstream). In this experiment, the depletion zone border shifted less than 700 µm in 1 h. A previous report on nanofluidic concentration devices indicated a near-zero shift after 3 h of actuation[28], although under different experimental conditions, indicating that the result reported here could be further optimized. However, the near-stability of the isotachophoretic separations demonstrated here greatly enhances monitoring of focusing and separation processes by microscopy without *x*/*y*control of the microscope stage. Additionally, the experimental time range is much larger than for nonstationary ITP methods, allowing higher concentration factors to be achieved.
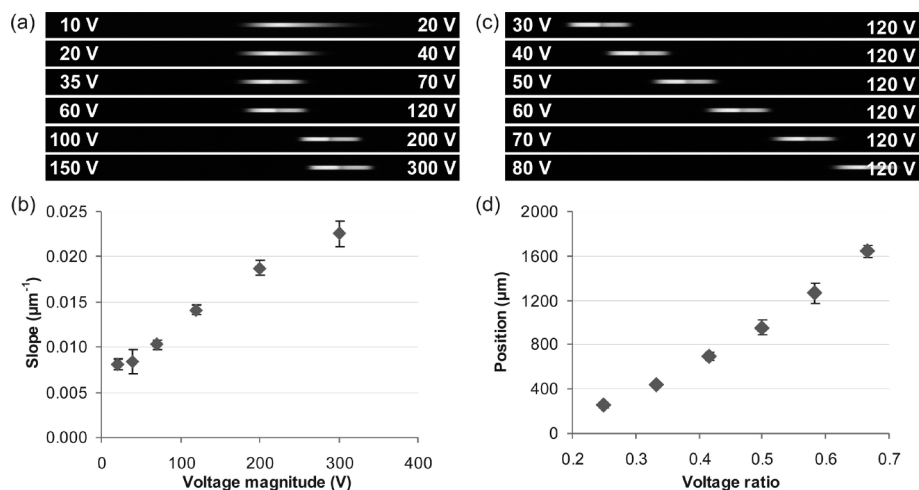
Figure 4. Three-point voltage actuation. (a) Focusing and separation of fluorescein and 6-carboxyfluorescein at several voltage magnitudes. (b) Dependence of focusing strength on the voltage magnitude. Focusing strengths are represented by the steepness of the slopes between the fluorescein plateau and the depletion zone; voltage magnitudes are represented by the upstream voltage. (c) Fluorescein and 6-carboxyfluorescein zones at different ratios between upstream and downstream voltages. (d) Distances of the edge between the depletion zone and the fluorescein zone from the nanochannel. Measurements were triplicated and randomized.

Three-Point Voltage Actuation

In Figure 4 we demonstrate the versatility that is provided by a three-point voltage actuation approach. In Figure 4a,b the magnitude of the upstream and downstream voltages was varied, while maintaining the ratio between them. This enables tuning of the extent to which analytes are focused. For low voltages the two zones are barely distinguishable, while for high voltages sharp edges of the zones can be observed. Figure 4b shows normalized slope values in fluorescence intensity per micrometer. The results suggest a linear trend between voltage magnitude and zone sharpness. Analyte zone positions are not greatly influenced by a change of the voltage magnitude as long as the

ratio between upstream and downstream voltages is kept constant. In principle, this enables a free choice of the maximum field strength and resulting focusing strength. However, small shifts in analyte zone positions are observed at higher voltage magnitudes. We measured maximum shifts of 364 ± 21 µm.

In Figure 4c,d the voltage ratio is varied by means of the downstream voltage. The zones can be shifted over a range of 1.4 mm by varying the voltage ratio between 0.25 and 0.67 (downstream voltage: upstream voltage). Zone positions appear to relate rather linearly to the voltage ratio. Separations are maintained, although at increasing ratios defocusing occurs. The 1.4 mm zone shift is accompanied by a decrease of slope values on the order of 0.006 µm–1.

Complete control over analyte zone position and sharpness is a crucial and unique advantage of dzITP over conventional ITP methods. In conventional methods, a single stable position can be obtained by EOF balancing, but during the experiment this position can not be easily changed without changing parameters like pH or electrolyte concentrations. Contrarily, in dzITP this is easily done by tuning the upstream and downstream voltage magnitudes. Real-time image analysis of fluorescent markers can be used as feedback input for three-point voltage actuation, enabling automated zone positioning control. Moreover, great benefit is offered to experimental readout, as analyte zones can be scanned in a precisely controllable manner by steering them along a sensor.

Synergy of dzITP

Table 1 summarizes the synergy that emerges from the combination of ITP and nanofluidic concentration devices, as provided by dzITP. Except for the

requirement of multiple electrolytes, dzITP has all key characteristics of ITP: focusing toward plateau concentrations and separation into adjacent zones that are ordered according to ionic mobility. Spacer compounds can be used to segregate adjacent zones. From nanofluidic concentration devices, dzITP takes the single-electrolyte advantage, as well as positional stability. Three-point voltage actuation adds to this synergy the possibility of precise control of focusing strength and zone positioning.

Table 1. Comparison of dzITP with Conventional ITP Methods and Nanofluidic Concentration Devices (NCD). v = intrinsic or standard possibility; – = not possible or not demonstrated in literature; m = possible with modification.

property	ITP	NCD	dzITP
analyte focusing	v	v	v
separation of ions	v	–	v
spacer insertion	v	–	v
single electrolyte	–	v	v
near-stationary	m	v	v
voltage-controlled zone positioning	–	–	v

Conclusion and Outlook

In this paper we have demonstrated isotachophoretic separations employing a nanochannel-induced depletion zone as a trailing electrolyte. dzITP requires only a single electrolyte to be injected and can be performed easily with both discrete and continuous injections. We demonstrated separations of up to four compounds in clearly distinguishable zones within 100 s. A spacer was inserted to improve baseline separation of fluorescent compounds, and to induce selective transport of analytes while maintaining sharply focused zones. Moreover, full control over analyte position and zone sharpness was demonstrated using the unique three-point voltage control of dzITP.

Scanning of analyte zones using three-point voltage actuation will enable simple integration of sensors such as surface-enhanced Raman spectroscopy (SERS), surface plasmon resonance (SPR), and conductimetry or electrochemical detection. As dzITP is much easier to use than conventional ITP, integration into a microfluidic platform for everyday laboratory use will be very attractive, as exemplified by the Agilent 2100 Bioanalyzer for on-chip capillary electrophoresis. Integration in hand-held analysis devices, as has been recently done for conventional ITP,[18] may find interesting applications in water quality monitoring, explosive detection, point-of-care screening, etc. Future research focuses on coupling of the technique to sampling and detection modules. We see great potential for dzITP in our metabolomics research, particularly for the extraction, preconcentration, and quantification of low-abundant metabolites from small complex biological samples. Thanks to its unique combination of voltage-controlled versatility and single-electrolyte simplicity, dzITP holds the promise to become a core component in the electrokinetic chip-based platforms of the future.

References

1. L. Chen, J. E. Prest, P. R. Fielden, N. J. Goddard, A. Manz and P. J. R. Day, Lab on a Chip **6** (4), 474-487 (2006).
2. S. M. Kenyon, M. M. Meighan and M. A. Hayes, Electrophoresis **32** (5), 482-493 (2011).
3. P. A. Walker, M. D. Morris, M. A. Burns and B. N. Johnson, Analytical Chemistry **70** (18), 3766-3769 (1998).
4. D. Kaniansky, M. Masár, J. Bielčiková, F. Iványi, F. Eisenbeiss, B. Stanislawski, B. Grass, A. Neyer and M. Jöhnck, Analytical Chemistry **72** (15), 3596-3604 (2000).
5. D. Bottenus, T. Z. Jubery, Y. Ouyang, W.-J. Dong, P. Dutta and C. F. Ivory, Lab on a Chip **11** (5), 890-898 (2011).
6. D. Bottenus, T. Z. Jubery, P. Dutta and C. F. Ivory, Electrophoresis **32** (5), 550-562 (2011).

7. J. Wang, Y. Zhang, M. R. Mohamadi, N. Kaji, M. Tokeshi and Y. Baba, Electrophoresis **30** (18), 3250-3256 (2009).
8. B. Jung, R. Bharadwaj and J. G. Santiago, Analytical Chemistry **78** (7), 2319-2327 (2006).
9. M. Bercovici, G. V. Kaigala, C. J. Backhouse and J. G. Santiago, Analytical Chemistry **82** (5), 1858-1866 (2010).
10. J. E. Prest, M. S. Beardah, S. J. Baldock, S. P. Doyle, P. R. Fielden, N. J. Goddard and B. J. T. Brown, Journal of Chromatography A **1195** (1–2), 157-163 (2008).
11. H. Huang, F. Xu, Z. Dai and B. Lin, Electrophoresis **26** (11), 2254-2260 (2005).
12. D. Liu, Z. Ou, M. Xu and L. Wang, Journal of Chromatography A **1214** (1–2), 165-170 (2008).
13. D. Liu, M. Shi, H. Huang, Z. Long, X. Zhou, J. Qin and B. Lin, Journal of Chromatography B **844** (1), 32-38 (2006).
14. A. Persat, L. A. Marshall and J. G. Santiago, Analytical Chemistry **81** (22), 9507-9511 (2009).
15. R. B. Schoch, M. Ronaghi and J. G. Santiago, Lab on a Chip **9** (15), 2145-2152 (2009).
16. A. Persat and J. G. Santiago, Analytical Chemistry **83** (6), 2310-2316 (2011).
17. M. Bercovici, G. V. Kaigala, K. E. Mach, C. M. Han, J. C. Liao and J. G. Santiago, Analytical Chemistry **83** (11), 4110-4117 (2011).
18. G. V. Kaigala, M. Bercovici, M. Behnam, D. Elliott, J. G. Santiago and C. J. Backhouse, Lab on a Chip **10** (17), 2242-2250 (2010).
19. L. Suntornsuk, Anal Bioanal Chem **398** (1), 29-52 (2010).
20. A. García-Campaña, L. Gámiz-Gracia, F. Lara, M. Olmo Iruela and C. Cruces-Blanco, Anal Bioanal Chem **395** (4), 967-986 (2009).
21. F. E. Ahmed, Journal of Chromatography B **877** (22), 1963-1981 (2009).
22. M. Urbánek, A. Varenne, P. Gebauer, L. Křivánková and P. Gareil, Electrophoresis **27** (23), 4859-4871 (2006).
23. M. C. Breadmore, Journal of Chromatography A **1217** (24), 3900-3906 (2010).
24. M. C. Breadmore, Electrophoresis **29** (5), 1082-1091 (2008).
25. M. C. Breadmore and J. P. Quirino, Analytical Chemistry **80** (16), 6373-6381 (2008).
26. G. I. Abelev and E. R. Karamova, Molecular Immunology **26** (1), 41-47 (1989).
27. S. M. Kim, M. A. Burns and E. F. Hasselbrink, Analytical Chemistry **78** (14), 4779-4785 (2006).
28. Y.-C. Wang, A. L. Stevens and J. Han, Analytical Chemistry **77** (14), 4293-4299 (2005).
29. S. J. Kim, Y.-A. Song and J. Han, Chemical Society Reviews **39** (3), 912-922 (2010).

30. J. Astorga-Wells, S. Vollmer, S. Tryggvason, T. Bergman and H. Jörnvall, Analytical Chemistry **77** (22), 7131-7136 (2005).
31. S.-R. Park and H. Swerdlow, Analytical Chemistry **75** (17), 4467-4474 (2003).
32. A. Plecis, R. B. Schoch and P. Renaud, Nano Letters **5** (6), 1147-1155 (2005).
33. K. G. H. Janssen, H. T. Hoang, J. Floris, J. de Vries, N. R. Tas, J. C. T. Eijkel and T. Hankemeier, Analytical Chemistry **80** (21), 8095-8101 (2008).
34. T. A. Zangle, A. Mani and J. G. Santiago, Analytical Chemistry **82** (8), 3114-3117 (2010).
35. T. A. Zangle, A. Mani and J. G. Santiago, Chemical Society Reviews **39** (3), 1014-1035 (2010).
36. Q. Pu, J. Yun, H. Temkin and S. Liu, Nano Letters **4** (6), 1099-1103 (2004).
37. Q. Yu and Z. Silber-Li, Microfluid Nanofluid **11** (5), 623-631 (2011).
38. K.-D. Huang and R.-J. Yang, Electrophoresis **29** (24), 4862-4870 (2008).
39. H. Yu, Y. Lu, Y.-g. Zhou, F.-b. Wang, F.-y. He and X.-h. Xia, Lab on a Chip **8** (9), 1496-1501 (2008).
40. X. Mao, B. R. Reschke and A. T. Timperman, Electrophoresis **31** (15), 2686-2694 (2010).
41. B. Scarff, C. Escobedo and D. Sinton, Lab on a Chip **11** (6), 1102-1109 (2011).
42. D. Wu and A. J. Steckl, Lab on a Chip **9** (13), 1890-1896 (2009).
43. K. Zhou, M. L. Kovarik and S. C. Jacobson, Journal of the American Chemical Society **130** (27), 8614-8616 (2008).
44. J. H. Lee, Y.-A. Song, S. R. Tannenbaum and J. Han, Analytical Chemistry **80** (9), 3198-3204 (2008).
45. J. Lee and J. Han, Microfluid Nanofluid **9** (4-5), 973-979 (2010).
46. L. F. Cheow, S. H. Ko, S. J. Kim, K. H. Kang and J. Han, Analytical Chemistry **82** (8), 3383-3388 (2010).
47. Y.-C. Wang and J. Han, Lab on a Chip **8** (3), 392-394 (2008).
48. J. H. Lee, B. D. Cosgrove, D. A. Lauffenburger and J. Han, Journal of the American Chemical Society **131** (30), 10340-10341 (2009).
49. A. Sarkar and J. Han, Lab on a Chip **11** (15), 2569-2576 (2011).
50. S. H. Ko, S. J. Kim, L. F. Cheow, L. D. Li, K. H. Kang and J. Han, Lab on a Chip **11** (7), 1351-1358 (2011).
51. J. H. Lee, Y.-A. Song and J. Han, Lab on a Chip **8** (4), 596-601 (2008).
52. S. J. Kim, S. H. Ko, K. H. Kang and J. Han, Nat Nano **5** (4), 297-301 (2010).
53. S. J. Kim, L. D. Li and J. Han, Langmuir **25** (13), 7759-7765 (2009).